J. Iron Steel Res. Int. (2020) 27:842–848
https://doi.org/10.1007/s42243-020-00396-y

ORIGINAL PAPER

Microstructure and properties of hybrid additive manufacturing 316L component by directed energy deposition and laser remelting

Xiao-hui Chen[1,2] · Bo Chen[1] · Xu Cheng[1] · Guo-chao Li[1] · Zheng Huang[1]

Received: 14 May 2019 / Revised: 17 August 2019 / Accepted: 25 August 2019 / Published online: 22 April 2020
© China Iron and Steel Research Institute Group 2020

Abstract
Arc additive manufacturing is a high-productivity and low-cost technology for directly fabricating fully dense metallic components. However, this technology with high deposit rate would cause degradation of dimensional accuracy and surface quality of the metallic component. A novel hybrid additive manufacturing technology by combining the benefit of directed energy deposition and laser remelting is developed. This hybrid technology is successfully utilized to fabricate 316L component with excellent surface quality. Results show that laser remelting can largely increase the amount of δ phases and eliminate σ phases in additive manufacturing 316L component surface due to the rapid cooling. This leads to the formation of remelting layer with higher microhardness and excellent corrosion resistance when compared to the steel made by directed energy deposition only. Increasing laser remelting power can improve surface quality as well as corrosion resistance, but degrade microhardness of remelting layer owing to the decrease in δ phases.

Keywords Hybrid additive manufacturing · Laser remelting · Directed energy deposition · Microstructure · Corrosion resistance

1 Introduction

Additive manufacturing (AM) combines welding technique with advanced rapid prototyping to directly fabricate fully dense metallic components. This technology has emerged as a viable means for high efficiency and low cost [1, 2]. It utilizes a heat source (e.g., laser, arc and electron beam) to melt metal wire or powder by layered manufacturing metallic components from a computer-aided design model [3–5]. In comparison with traditional manufacturing technologies, AM is particularly attractive for manufacturing and repairing complicated metallic components due to low production cycle and cost, high material utilization ratio and excellent processing flexibility [6, 7].

Compared with other AM technologies, arc additive manufacturing has advantages of high productivity, low cost and powerful bonding strength of components [8]. However, excess residual heat delays solidification under high deposit rate, causing degradation of dimensional accuracy and mechanical properties of the metallic component [9]. Spencer et al. [10] stated that the surface finishing of AM components can be improved by carefully controlling the temperature of parts. Doumanidis and Kwak [11–13] monitored and controlled process parameters for improving the dimensional accuracy, surface flatness and properties of AM components. However, the effects of those technologies are limited by high deposit rate.

A novel hybrid additive manufacturing (HAM) technology that combines directed energy deposition (DED) with laser remelting (LR) is developed in this paper. This hybrid technology utilizes DED to fabricate metal components with high deposit rate (more than 5 kg h^{-1} for steel), as well as LR to remelt the rough surface of the component to improve surface flatness and material properties. LR is a low-cost, low-complexity and highly repeatable surface treatment technique that produces a refined

✉ Xu Cheng
chengxu@buaa.edu.cn

[1] National Engineering Laboratory of Additive Manufacturing for Large Metallic, Components and Engineering Research Center, Ministry of Education on Laser Direct Manufacturing for Large Metallic Components, School of Materials Science and Engineering, Beihang University, Beijing 100191, China

[2] Research Center for Processing, AECC Shanghai Commercial Aircraft Engine Manufacturing Co., Ltd., Shanghai 201306, China

microstructure with significantly improved surface properties. And it is successfully applied for various metallic materials, such as titanium alloy and steel [14–20]. DED process is characterized by high-temperature gradients, low cooling rates and cycling reheating [21, 22], and LR process is characterized by rapid solidification and cooling [14]. The hybrid additive manufacturing by DED and LR would cause large differences in microstructures and properties from components made by traditional manufacturing routes.

The alloy studied in the present paper is 316L stainless steel, which is widely used in modern industries such as chemistry productions, steamship buildings, high-temperature bolts and nuclear reactors [23–25]. The microstructure of this austenitic stainless steel is very sensitive to the thermal history; therefore, the different microstructures such as delta ferrite (δ), sigma (σ) and austenite (γ) can be obtained. In this paper, the surface morphology, microstructure evolution and properties of HAM 316L stainless steel are investigated with the discussion of mechanisms.

2 Experimental

2.1 Material fabrication

HAM system consists of a Fronius TPS 5000 arc power source, an IPG YLS-10000 laser device, a six-axis KUKA robot and an argon-purged deposition chamber. A thick plate with a geometric size of 160 mm × 50 mm × 30 mm was deposited by this system. The process parameters of HAM are given in Table 1. Schematic illustration of HAM is shown in Fig. 1. The adjacent scanning tracks were opposite with the spacing of 8 mm (Fig. 1a). Twenty-five layers were deposited with the height of 2.5 mm and the time interval of 1 min. The surface of the component is smooth when using laser remelting technology with the scanning direction parallel to deposition direction (Fig. 1b). The spacing between two adjacent laser tracks was 5 mm. 316L wire with the diameter of 1.2 mm was employed as the starting material, and the chemical composition (wt.%) is given in Table 2. HAM process was executed in a specifically designed processing chamber with the contents of oxygen less than 0.008%.

Table 1 Process parameters of HAM

DED process				
Current/A	Voltage/V	Scan rate/(mm min^{-1})	Wire feed rate/(m min^{-1})	Deposit rate/(kg h^{-1})
300	28	600	10	5.3
LR process				
Laser power/kW		Scan rate/(mm min^{-1})	Spot diameter/mm	
4		500	5	
8		500	5	

2.2 Microstructure characterization

The specimens of HAM 316L component were prepared by standard mechanical polishing for metallographic microstructure analysis. A mixture solution (4 g $CuSO_4$, 20 mL HCl and 20 mL H_2O) was used as the etching agent. LR and DED microstructure of HAM 316L stainless steel was examined through the Olympus BX51M optical microscope (OM). The electron backscattered diffraction (EBSD) for observation and identification of δ and σ phases was equipped in a FEI NANO SEM 430 scanning electron microscope (SEM). The working distance of EBSD was 0.08–0.30 μm. Image-Pro Plus software was used to estimate the phase volume percentages.

2.3 Microhardness tests

A HXZ-1000 semi-automatic Vicker tester was used to measure microhardness. The test load is 5 N with 10-s dwell time. Five points of the same area were tested for an average.

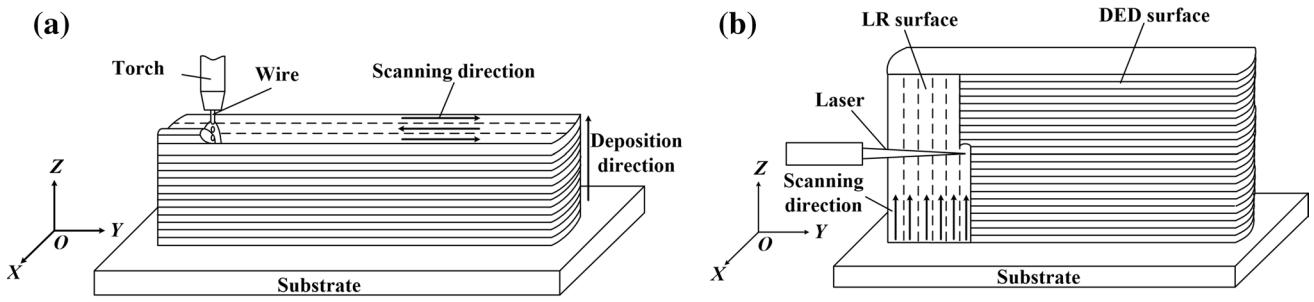

Fig. 1 Schematic illustration of HAM. **a** DED process; **b** LR process

Table 2 Chemical composition of HAM 316 component (wt.%)

C	Cr	Ni	Mo	Si	Mn	P	Cu	Fe
0.014	18.74	11.82	2.67	0.56	1.55	0.03	0.17	Balance

2.4 Electrochemical tests

The electrochemical corrosion properties of HAM 316L stainless steel were determined using a CorrTest electrochemical workstation when immersed in a 3.5 wt.% NaCl solution at 25 °C. The platinum foil was used as the counter electrode. The potentials quoted are referred to the saturated calomel electrode (SCE). Nitrogen was bubbled with the rate of 0.15 L/min for half an hour before specimen immersion in order to reduce oxygen level. Each specimen was scanned potentiodynamically with the rate of 30 mV/min from 50 mV below open-circuit potential until the current density exceeded 10^{-4} A/cm^2. In this paper, the pitting potential (E_p) was defined as the potential at which a significant increase in current density appeared. The corrosion current density (i_{corr}) was calculated by the Tafel extrapolation method according to ASTM G102.

3 Results

3.1 Surface morphology

The surface and cross section of DED and HAM 316L components are presented in Figs. 2 and 3, respectively. 316L component fabricated by DED at the deposit rate of 5.3 kg h^{-1} exhibits irregular undulant surface, as shown in Fig. 3a, b. After laser remelting at 4 kW, this component forms uneven surface and fluctuant fusion line with the maximum depth of 2.2 mm, as shown in Fig. 3c, d. When the laser power increases to 8 kW, HAM component can achieve a flat surface with the maximum depth of 2.5 mm, as shown in Figs. 3e, f.

3.2 Microstructure

Figure 4 shows grain morphology of HAM 316L steel with the deposition rate of 5.3 kg h^{-1} and the laser power of 8 kW. A large number of directional columnar grains form in DED 316L. A prominent feature observed is grain structure reorientation on the remelted interface. The grains in LR 316L have a similar directional structure with DED 316L, but the size is smaller. SEM photograph and EBSD phase map (Fig. 5a–c) show that δ and σ phases exhibit vermicular morphology in γ matrix of DED 316L steel. δ phases in LR surface are thinner and closer as shown in Fig. 5d–f. No σ phase appears in LR surface due to rapid cooling rate during

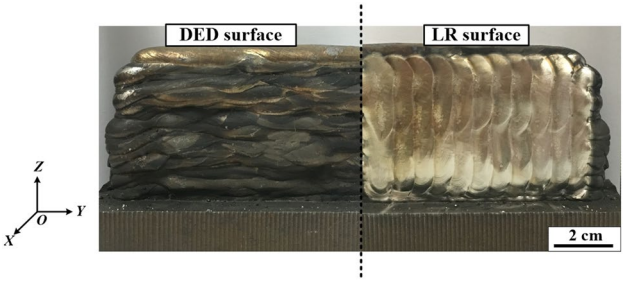

Fig. 2 Surface morphology of DED and HAM 316L components

LR process. LR microstructures at different laser powers are presented in Fig. 6. With the laser power increasing, the volume fraction of δ phase in LR surface reduces from 11.8 to 8.9 vol.% as shown in Table 3.

3.3 Microhardness

Figure 7 shows the microhardness of HAM 316L steel from the upper surface to bottom with a spacing of 0.2 mm. The average microhardness of DED steel and LR surfaces is given in Table 3. Compared with DED steel, LR surfaces have higher microhardness. With the laser power increasing, the microhardness of LR surface decreases from 224 to 214 HV. By contrast, the microhardness of 316L fabricated by selective laser melting (SLM) and laser metal deposition (LMD) is 213–220 HV [26] and 202–210 HV [27], respectively. The microhardness of casting 316L steel is 170–190 HV [28] which is lower than that of AM 316L steel, as shown in Fig. 7.

3.4 Corrosion properties

The corrosion properties of DED 316L and LR surfaces in a 3.5 wt.% NaCl solution are evaluated using a potentiodynamic polarization method, and the corresponding polarization curves are presented in Fig. 8. The measured values of the electrochemical parameters are given in Table 3. The low corrosion current density indicates a slow corrosion rate with high general corrosion resistance, and the high ΔE indicates high pitting corrosion resistance [29, 30]. Compared with DED steel, LR surface at 4 kW has higher i_{corr}. When the laser power increases to 8 kW, i_{corr} is lower than that of DED steel. LR layers show higher ΔE than DED steel, which means that LR process can improve the pitting corrosion resistance by eliminating σ phase.

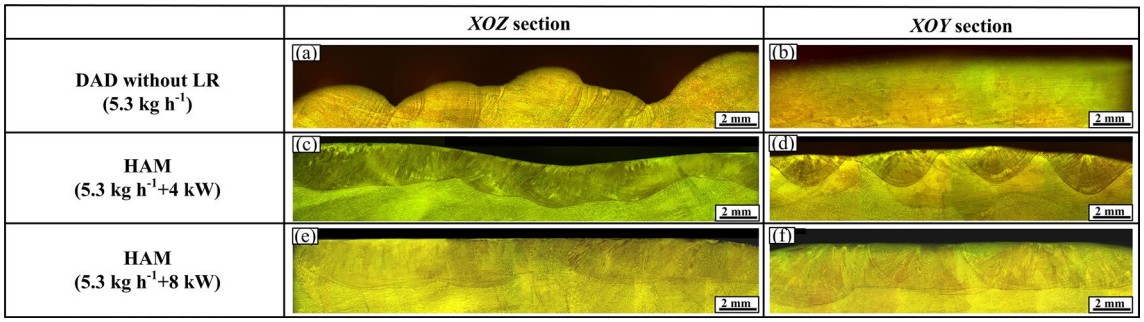

Fig. 3 *XOZ* (**a**, **c**, **e**) and *XOY* (**b**, **d**, **f**) sections of 316L components. **a**, **b** DED component (5.3 kg h^{-1}) without LR; **c**, **d** HAM component (5.3 kg h^{-1} + 4 kW); **e**, **f** HAM component (5.3 kg h^{-1} + 8 kW)

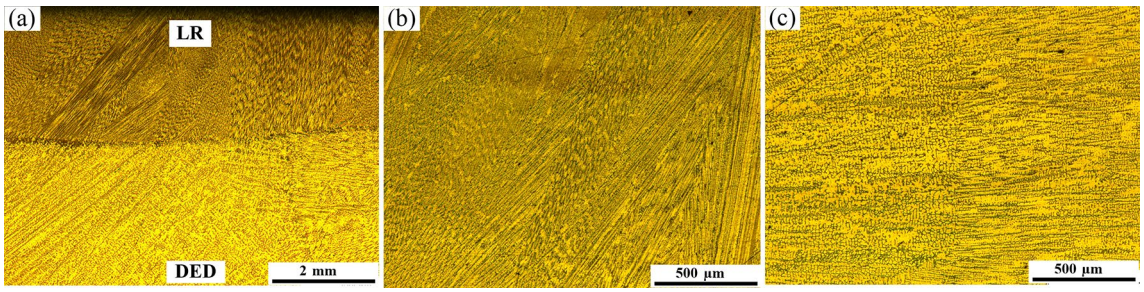

Fig. 4 Macrostructure photographs (*XOZ* section) of HAM 316L steel. **a** Low-magnification photograph; **b** high magnification of LR 316L; **c** high magnification of DED 316L

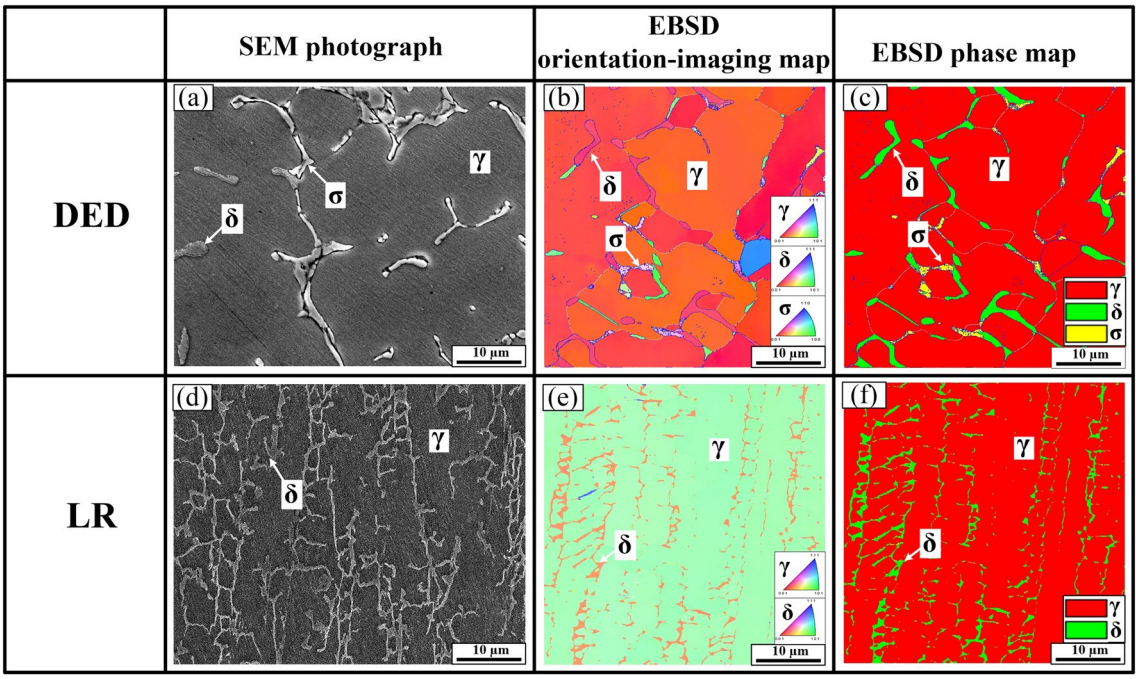

Fig. 5 Microstructure photographs (*XOZ* section) of HAM 316L component

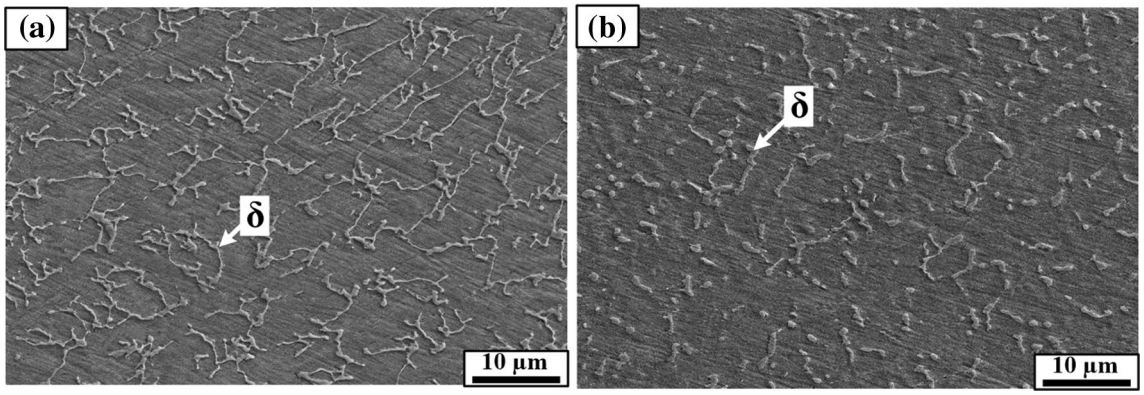

Fig. 6 Microstructure photographs (*YOZ* section) of LR surface at different laser powers. **a** 4 kW; **b** 8 kW

Table 3 Phase volume fraction, microhardness and electrochemical parameters of DED 316L and LR surface

Sample	δ phase/vol.%	σ phase/vol.%	Microhardness/HV	i_{corr}/(A cm^{-2})	E_{corr}/V$_{SCE}$	E_p/V$_{SCE}$	ΔE/V$_{SCE}$
DED	7.8	3.0	202	7.8×10^{-8}	− 0.15	0.47	0.62
LR at 4 kW	11.8	0	224	11.1×10^{-8}	− 0.14	0.65	0.79
LR at 8 kW	8.9	0	214	6.7×10^{-8}	− 0.17	0.70	0.87

E_{corr} Corrosion potential; $\Delta E = E_p - E_{corr}$

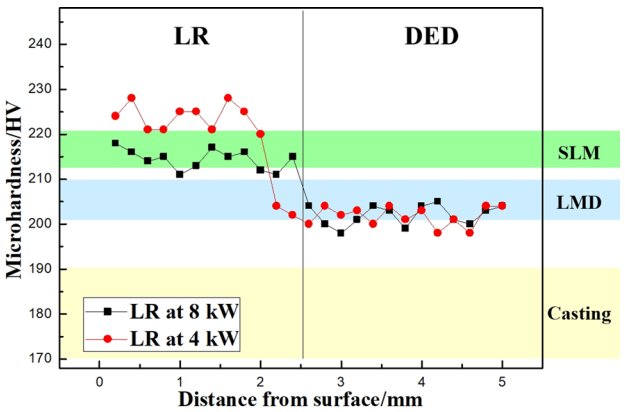

Fig. 7 Microhardness of 316L components fabricated by HAM, SLM, LMD and casting

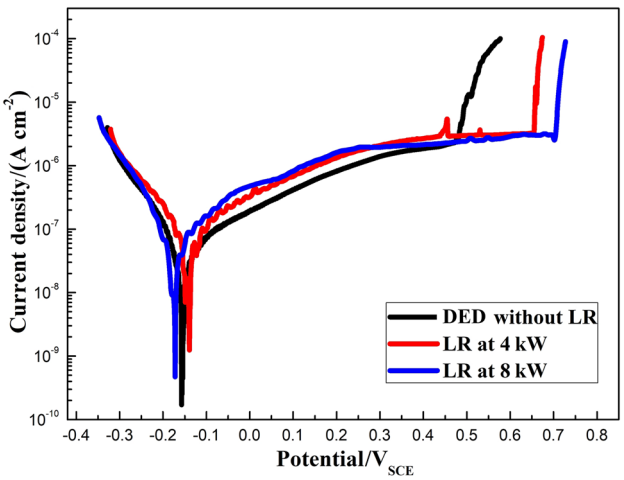

Fig. 8 Potentiodynamic curves of DED 316L and LR surface in 3.5% NaCl solution at 25 °C

4 Discussion

DED and LR processes are both characterized by directional solidification, leading to the columnar grain structure. The grain structure reorientates on the remelted interface because the temperature gradient of these two processes is orthogonal. In DED process, heat accumulation of previously deposited layers and heat input of subsequent layers could slow down the cooling rate of the components. Compared with the cooling rate of DED process (10^1–10^2 K/s), the cooling rate of LR process (10^2–10^6 K/s) is much higher owing to rapid heat dissipation through cold substructure, resulting in different microstructures between DED and LR processes.

During solidification, dendritic δ phase generates preferentially along the opposite direction of the temperature gradient in DED 316L steel. Then, at the cooling process, δ phase continuously transforms into γ phase (solid-state

transformation). As to cycling reheating and slow cooling during DED process, the temperature of steel can be maintained in δ/γ transformation region for a certain period of time, resulting in a large portion of δ phase dissolving in γ matrix with only a few vermicular δ phases retaining. Meanwhile, σ phase forms at the interface of δ/γ region with similar morphology as δ phase. Thus, δ and σ phases exhibit vermicular morphology within γ matrix in DED steel (Fig. 5a). The cooling rate of LR process is faster than that of DED process, and there is no subsequent thermal cycle effect. The shorter cooling time further limits diffusion-controlled transformation from δ to γ phase. Thus, more δ phase that exhibits vermicular morphology is retained in LR layer than in DED steel (Fig. 5b–f). Meanwhile, σ phase is eliminated by fast cooling during LR process. Increasing laser power would reduce the cooling rate of LR process that increases the holding time at the temperature of δ/γ transformation, leading to the volume fraction of δ phase reduction (Fig. 6). The microstructure morphology of AM 316L steel depends on the cooling rate. In other AM processes with slow cooling rate, such as selective electron beam melting [31], the microstructure displays δ and σ phases which are similar to that in DED steel. When 316L steel is fabricated by LMD [27, 32] and SLM [26] processes that have rapid cooling rate, only δ phase forms like that in LR layer.

It is well accepted and understood that δ phase, as well as σ phase, in austenitic stainless steel acts as a strengthening phase [33]. Although LR process eliminates σ phase, a large amount of δ phase replacing σ phase plays an important role in the strengthening of the steel. Thus, LR layer shows higher microhardness than DED steel. With the increases in laser power, the microhardness of LR layer reduces owing to that the volume fraction of δ phase decreases (Fig. 6 and Table 3). The microhardness results of DED 316L are in accordance with those of other AM 316L steel because of similar microstructure. In contrast to casting 316L steel, AM 316L steel consists of finer grains and more δ phases, leading to higher microhardness.

Since δ phase contains the high amount of Cr elements, and the interface around it is similarly depleted in Cr as σ phase, Cr-depleted region is sensitive to corrosion attack and more prone to pitting corrosion. Previous research indicates that σ phase has a much more detrimental effect on degradation of pitting corrosion resistance than δ phase [34]. Consequently, LR process can improve the pitting corrosion resistance of surface on DED steel by eliminating σ phase although δ phase increases. Since δ and σ phases within γ matrix produce galvanic corrosion in austenitic stainless steel, reducing the volume fraction of δ by increasing laser power can improve the corrosion resistance of LR surface.

5 Conclusions

1. LR can increase δ phase and eliminate σ phase due to rapid cooling, forming a LR layer with higher microhardness and pitting corrosion resistance than DED steel.
2. Increasing laser power can improve corrosion resistance by reducing volume fraction of δ phase and eliminating σ phase, but degrade the microhardness of surface.

Acknowledgements This work was supported by Beijing Municipal Science & Technology Program (Grant No. Z181100003318001).

References

[1] W.E. Frazier, J. Mater. Eng. Perform. 23 (2014) 1917–1928.
[2] H.M. Wang, S.Q. Zhang, X.M. Wang, Chin. J. Lasers 36 (2009) 3204–3209.
[3] J. Xiong, G.J. Zhang, J. Mater. Process. Technol. 214 (2014) 962–968.
[4] M. Katou, J. Oh, Y. Miyamoto, K. Matsuura, M. Kudoh, Mater. Des. 28 (2007) 2093–2098.
[5] B. Baufeld, O. van der Biest, R. Gault, K. Ridgway, IOP Conference Series: Materials Science and Engineering, IOP Publishing, Britain, UK, 2011.
[6] X. Yan, P. Gu, Comput. Aid. Des. 28 (1996) 307–318.
[7] D. Clark, M.R. Bache, M.T. Whittaker, J. Mater. Process. Technol. 203 (2008) 439–448.
[8] M.P. Mughal, H. Fawad, R.A. Mufti, Proc. Inst. Mech. Eng. Part C J. Mech. Eng. Sci. 220 (2006) 875–885.
[9] X.H. Chen, J. Li, X. Cheng, B. He, H.M. Wang, Z. Huang, Mater. Sci. Eng. A 703 (2017) 567–577.
[10] J.D. Spencer, P.M. Dickens, C.M. Wykes, Proc. Inst. Mech. Eng. Part B J. Eng. Manuf. 212 (1998) 175–182.
[11] C. Doumanidis, Y.M. Kwak, J. Manuf. Sci. Eng. 123 (2001) 45–52.
[12] C. Doumanidis, Y.M. Kwak, Int. J. Pressure Vessels Piping 79 (2002) 251–262.
[13] Y.M. Kwak, C.C. Doumanidis, J. Manuf. Process. 4 (2002) 28–41.
[14] N. Cheung, M.A. Larosa, W.R.R. Osório, M.C.F. Lerardi, A. Garcia, Adv. Mater. Res. 59 (2008) 1119–1124.
[15] E. Chikarakara, S. Naher, D. Brabazon, Surf. Coat. Technol. 206 (2012) 3223–3229.
[16] Y. Hua, Y. Bai, Y. Ye, Q. Xue, H. Liu, R. Chen, K. Chen, Appl. Surf. Sci. 283 (2013) 775–780.
[17] C. Wang, H. Zhou, N. Liang, C. Wang, D. Cong, C. Meng, L. Ren, Appl. Surf. Sci. 313 (2014) 333–340.
[18] J. Yao, Q. Zhang, M. Gao, W. Zhang, Appl. Surf. Sci. 254 (2008) 7092–7097.
[19] E. Chikarakara, S. Naher, D. Brabazon, Appl. Surf. Sci. 302 (2014) 318–321.
[20] B. Zbigniew, M. Bonek, L.A. Dobrzański, D. Ugues, M.A. Grande, Mater. Sci. Forum 654–656 (2010) 2511–2514.
[21] H. Zhao, G. Zhang, Z. Yin, L. Wu, J. Mater. Process. Technol. 211 (2011) 488–495.
[22] V.D. Fachinotti, A. Cardona, B. Baufeld, O. Van der Biest, Acta Mater. 60 (2012) 6621–6630.
[23] R.B. Song, J.Y. Xiang, D.P. Hou, J. Iron Steel Res. Int. 18 (2011) No. 11, 53–59.

[24] M.M. Ma, Z.M. Wang, D.Z. Wang, X.Y. Zeng, Opt. Laser Technol. 45 (2013) 209–216.
[25] F.X. Xie, X.B. He, S.L. Cao, X.H. Qua, J. Mater. Process. Technol. 213 (2013) 838–843.
[26] Z. Sun, X. Tan, B.S. Tor, W.Y. Yeong, Mater. Des. 104 (2016) 197–204.
[27] X. Xu, G.Y. Mi, Y.Q. Luo, P. Jiang, X.Y. Shao, C.M. Wang, Opt. Laser Eng. 94 (2017) 1–11.
[28] M. Nan, Microstructure and mechanical properties of welded joint of 316L stainless steel, Harbin Institute of Technology, Harbin, China, 2012.
[29] I. AghaAli, M. Farzam, M.A. Golozar, I. Danaee, Mater. Des. 54 (2014) 331–341.
[30] C.M. Lin, H.L. Tsai, C.D. Cheng, C. Yang, Eng. Fail. Anal. 21 (2012) 9–20.
[31] C. Wang, X. Tan, E. Liu, B.S. Tor, Mater. Des. 147 (2018) 157–166.
[32] A. Yadollahi, N. Shamsaei, S.M. Thompson, D.W. Seely, Mater. Sci. Eng. A 644 (2015) 171–183.
[33] W. Delong, Weld. J. 53 (1974) 273–286.
[34] X.H. Chen, J. Li, X. Cheng, H.M. Wang, Z. Huang, Mater. Sci. Eng. A 715 (2017) 307–314.